# Chain Diffusion in Ultralong *n*-Alkane Crystals Studied by $^{13}C$ NMR

**Philip G. Klein* and Martin A. N. Driver**

*IRC in Polymer Science and Technology, University of Leeds, Leeds, West Yorkshire, LS2 9JT, United Kingdom*

*Received March 30, 2000*

ABSTRACT: $^{13}C$ NMR progressive saturation measurements were used to investigate longitudinal relaxation in the crystal phase of semicrystalline alkanes. Novel monodisperse, ultralong *n*-alkanes were melt crystallized in such a way that they comprised crystals containing extended chains or once-folded chains. The crystalline morphology was confirmed using DSC, SAXS, and WAXS. Quantifying the longitudinal relaxation is critically dependent on an accurate measure of the crystallinity of the sample. Crystallinities were measured using X-ray scattering, calorimetric, and $^1H$ broadline NMR techniques. The longitudinal relaxation is interpreted via a solid-state chain diffusion process. Very high crystallinity was shown to suppress the diffusion. A one-dimensional diffusion model with a single reptation time was shown to represent successfully the relaxation of crystals comprising extended chains. The addition of chain folds was shown to result in a decrease in the diffusion coefficient, although the addition of branches at the fold surface did not represent a further constraint to diffusion. A dual reptation time diffusion model was developed and shown to describe successfully the relaxations of the crystals comprising folded chains. The diffusion coefficients were consistent with those previously measured for polyethylene, as was an estimate of the thickness of the interfacial region yielded by the diffusion model. The results were also analyzed using a conventional, multicomponent $T_1$ model, which suggested the crystalline $T_1$ may make a significant contribution at longer times. This explained the 100% relaxation seen for some samples.

## Introduction

Polyethylene is semicrystalline in the solid state, and the nature of the crystalline morphology exerts a large influence on its material properties.[1] For example, as crystallinity is increased, polyethylene becomes less sensitive to wide variations of stiffness with temperature.[2,3] The crystal regions are also much stiffer than the amorphous regions and are mechanically anisotropic,[1] making the orientation of the crystallites critically important. Correspondingly, commercial polyethylenes often undergo processing which tries to optimize the crystalline morphology to yield the desired characteristics.[1] Controlling the efficacy of these processes are the molecular dynamics which influence crystallization, lamellar thickening, and the enhancement of orientation. The purpose of this work is to investigate one such dynamic process: the exchange of material between the crystalline and amorphous phases as a result of crystalline chain diffusion. We shall do this by studying the $^{13}C$ longitudinal relaxation in a series of monodisperse *n*-alkanes, of various chain lengths, where the crystals are demonstrated to comprise fully extended or once-folded chains. The longitudinal relaxation is measured over a time period of 1200 s. After this time, most samples exhibited between 60 and 100% magnetization recovery, although extended chain samples only recovered to 20%. The results will be interpreted via a diffusion model and, for comparative purposes, a conventional $T_1$ model, where $T_1$ values are obtained from a double-exponential fit to the partially recovered magnetization.

Although the experimental observation of solid-state chain diffusion in polyethylene is not new, it is still a matter of some contention, especially regarding the extent of diffusion, and it is worthwhile reviewing the literature in this area. Crystalline chain diffusion was first observed in the seminal work of Ungar and Keller,[4] who observed intermixing of separate macroscopic crystals of long-chain paraffin molecules between 26 and 36 carbons in length. This mixing led to a new crystalline phase detectable by WAXS and calorimetry. Mixing of chains of the same lengths was demonstrated by deuterium labeling some of the alkanes, such that mixing of isotopically different chains changed the local molecular environment and hence could be detected with IR spectroscopy. Importantly, this work demonstrated that (a) chains within crystals diffuse in the solid state well below the melt and below the rotator phase; (b) the diffusion is long-range, covering distances (micrometers) far greater than the lengths of the diffusing chains (nanometers); (c) chains can gain access to, and diffuse into, solid macroscopic crystals; and (d) the driving force of the diffusion is not solely a result of the chains trying to increase their stem length within a crystal, as these alkanes were fully crystalline before the start of the experiment. Radiotracer, serial sectioning studies of self-diffusion[5] in C20 crystals showed long-range crystalline chain diffusion both parallel and perpendicular to the basal planes of the crystallites, which indicates that it is not necessary to have alkanes of different lengths for diffusion to occur. Annealing a purely mechanical mixture of microcrystals of two alkanes of slightly different lengths was shown to produce a mixed crystal.[6] This mixed crystal had the same properties as those obtained by co-crystallization of the two alkanes from solution. Here, a mechanism for the diffusion was proposed whereby molecules migrate substantially as all-trans rigid bodies. The authors also suggest that the chains move longitudinally along their axes, probably by rototranslational jumps. Yamamoto et al.[7,8] observed long-range crystalline diffusion in situ by optical microscopy. Diffusion was

10.1021/ma000571b CCC: $22.00 
Published on Web 07/11/2002

detected both transverse and longitudinal to the chain axis. Transverse diffusion shows the distance covered to be proportional to $t^{1/2}$, supporting a simple diffusional process. Longitudinal diffusion was more difficult to measure, since the molecules tended to diffuse into deep layers and then undergo transverse diffusion. Computer simulations[9] have demonstrated that torsional motions can couple with lattice vibrations to produce short-range twists in the chains (twist defects). These defects can move coherently toward the end of the crystal, thereby causing a chain diffusion process. Shorter alkanes diffuse via a collective twisting of the chains, which is not so strongly influenced by conformational defects. The alkanes used in the present work have been studied by a number of research groups. One such study[10] involving electron microscopy suggests that isothermal thickening of folded chains occurs through a solid-state diffusion process.

The evidence for chain diffusion from NMR experiments, based mainly on $^{13}C$ longitudinal relaxation, is more controversial, as it is hard to separate the contributions from physical diffusion of the chains and spin−lattice relaxation effects. Schmidt-Rohr and Spiess[11] used 2D exchange and $^{13}C$ experiments to clearly demonstrate that there is chain diffusion between crystalline and amorphous phases of polyethylene. The 2D experiments only lasted for a second or two for practical reasons, but they do show that chain diffusion does occur and provide no evidence to suggest that this diffusion should come to a halt after a particular time interval or diffused distance. NOE measurements also showed that the enhancement factors for the crystalline and amorphous phases are the same over the complete range of the $^{13}C$ relaxation, which indicates that the motions leading to these relaxations are the same for each phase. The frequency of these motions was calculated and shown to correspond to the amorphous phase. Hence, the magnetization in the crystalline phase is not generated by $^{13}C$ relaxation, but rather has been transported in from the amorphous phase. Similar $^{13}C$ relaxation measurements were carried out by Robertson et al.[12] on polyethylene samples subjected to controlled cross-linking by electron irradiation. A systematic decrease in the rate of recovery was observed with increasing amorphous phase cross-link density, which could not be explained through a conventional $T_1$ process, but was satisfactorily explained via a decrease in crystalline chain diffusion coefficient as a result of the hindrance to diffusion caused by cross-linking. Similar effects have been observed by Klein et al.[13] where the entanglement density has been varied via different annealing conditions. More recently, magic-angle turning and separated local field experiments[14] have shown that the principal values of the chemical shift tensor, and the local $^1H$ field of the tensor, for the all-trans crystalline structures with long and short $T_1$ are essentially the same. Thus, the local electronic and dipolar environments are the same, so different spin−lattice interactions cannot be the cause of the different $T_1$'s. This supports the suggestion that chain diffusion between the amorphous and crystalline regions in polyethylene is the primary reason for the multiexponential crystalline $T_1$ relaxations.

To gain a better understanding of the factors influencing crystalline chain diffusion in commercial polyethylenes, it would be ideal to study a system with an extremely well-characterized crystalline morphology which was comparable to the morphology in such materials. The short chain *n*-alkanes which have been previously studied[4−9] did not form folded chain crystals and were essentially single-phase systems with no amorphous component. Conversely, the studies of polyethylene[11−13] suffered from problems arising from their polydispersity. Since the materials contained chains of a range of different lengths, it was impossible to characterize fully the number of folds in each chain, the nature and tightness of those folds, or the amount of cilia and tie molecules present. The unique opportunity of studying crystalline chain diffusion in an exceptionally well-characterized, chain-folded two-phase system has now been made possible by the synthesis of ultralong monodisperse *n*-alkanes.

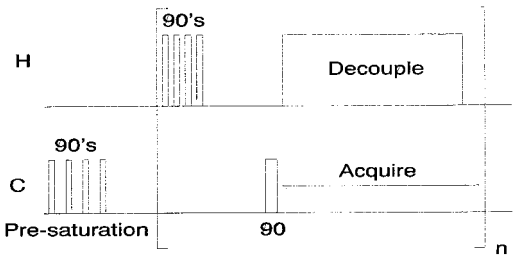


**Figure 1.** Progressive saturation pulse sequence used to measure the $^{13}C$ longitudinal relaxation.

These materials were first produced in the mid-1980s following the research work of Wegner[15] and that of Whiting[16] in an investigation aimed at the elucidation of the chain-folding crystallization process. Subsequently, Brooke and co-workers[17] at the University of Durham improved the method of Whiting and synthesized larger amounts of the linear alkanes $C_{198}H_{398}$, $C_{246}H_{494}$, and $C_{294}H_{590}$ and also produced the branched alkanes $C_{96}H_{193}CHRC_{94}H_{189}$ where R = $CH_3$ and $C_4H_9$, among other materials.

The monodispersity of these alkanes allows the crystals formed to be exceptionally well characterized. The alkane chains are long enough to crystallize by chain folding and comprise both crystalline and amorphous moieties.[18,19] The use of alkanes of differing molecular weight allows the study of crystals of different lamellar thicknesses with identical surrounding morphologies. Recent work on polyethylene studied materials of different lamellar thickness from 15 to 60 nm formed by pressure annealing,[13] but this could not be done without changing other aspects of the morphology, such as the fold surfaces and the entanglement density in the amorphous phase.[20] In the present work, precise control over the morphology of the alkane crystals provides a unique insight into the basic mechanism by which crystalline chain diffusion progresses.

## Experimental Section

**High-Resolution $^{13}C$ NMR.** Spectra were recorded on a Chemagnetics CMX-200, operating at 200 MHz for protons and 50.3 MHz for carbons. A progressive saturation pulse sequence was employed (Figure 1). A double-resonance MAS probe was used, and samples were spun at about 3.5 kHz. A 4 $\mu$s 90° pulse was used in the $^1H$ and $^{13}C$ channels, with a decoupling field strength equivalent to 82 kHz applied during the acquisition period. A series of FIDs were recorded, with a variation in the recycle delay time, $\tau_{rd}$, between 2 and 1200 s. All experiments were performed at 60 °C, as this temperature was believed to represent the ideal conditions for the observation of chain diffusion.[11]

The data lengths of the FIDs were doubled by zero filling, and the signal-to-noise was improved by multiplication of the FIDs by matched exponential filters.[21] The FIDs were then Fourier transformed into the frequency domain, where they were baseline corrected to a third-order polynomial.

**Wide-Line $^1$H NMR.** The probe had a 5 mm coil, and a 90° pulse width of 2 $\mu$s was used. A standard $90_x-\tau-90_y$ solid echo pulse sequence was used, with interpulse spacing, $\tau$, varying between 8 and 30 $\mu$s. The broad component of the spectrum, representing the crystalline phase, obtained at each value of $\tau$ was fitted to a modified Gaussian function.[12] The narrow component, representing the mobile amorphous phase, was fitted to a Lorentzian function. Each of these components decayed in a Gaussian manner as a function of $\tau$ and was extrapolated back to zero $\tau$, where the crystallinity was calculated as the fraction of the total signal associated with the modified Gaussian function.

**Differential Scanning Calorimetry (DSC).** DSC scans were carried out using a Perkin-Elmer DSC7, heating at 10 °C/min. The calorimeter was calibrated for temperature and energy from the melting behavior of two standards, indium and zinc, at 10 °C/min. The fractional crystallinity was measured by dividing the area of the melting endotherm, in J/g, by the 100% crystalline value, which for polyethylene is widely cited as 290 J/g.[22]

**Simultaneous Small- and Wide-Angle X-ray Scattering (SAXS and WAXS).** The X-ray scattering experiments reported in this paper were carried out at Station 8.2 of the Daresbury Synchrotron Radiation Source. The beamline was configured with an X-ray wavelength, $\lambda$, of 1.52 Å and a bandwidth $\Delta\lambda/\lambda \leq 4 \times 10^{-3}$. In the focal plane the beam size was $3 \times 0.3$ mm$^2$. Details of the storage ring, radiation, camera geometry, and data collection electronics can be found elsewhere.[23] The samples were placed in DSC pans containing 4 mm diameter windows made from 5 $\mu$m thick mica.

Small-angle scattered X-ray photons were detected on a quadrant multiwire position-sensitive detector[24] located 3.0 m from the sample. The calibration of the $q$ scale of the detector ($q = 4\pi \sin\theta/\lambda$, where the scattering angle is defined as $2\theta$) was performed using the first 25 orders of diffraction from wet rat tail collagen. A sixth-order polynomial was fitted to the inverse collagen spacings over the detector range. This corrects for the positional nonlinearity of the detector. All diffraction intensities were normalized by the beam flux which was monitored by an ionization chamber located behind the sample. Each of the SAXS scattering patterns was Lorentz corrected.[25]

Wide-angle X-ray scattered photons were detected utilizing a curved linear Inel delay line detector.[26] The detector was positioned such that its center of curvature coincided with the sample and such that it would not be an obstacle to the small-angle pattern. The scattering pattern of high-density polyethylene was used for the positional calibration of the detector. The experimental data were corrected for background scatter using the scatter from an empty sample holder and for nonuniform detector sensitivity using the response to a $^{58}$Fe X-ray source.

## Results and Discussion

**Sample Preparation and Characterization. (i) DSC Analysis**. Previous work by other authors on monodisperse alkanes has revealed that they show a preference for crystallizing with quantized fold length,[18,19] the crystals comprising either extended chains or chains completing almost exactly one, two, three, or four folds up to the longest chain examined, $C_{390}H_{782}$. This quantization leads to discontinuities in the dissolution temperature. Figure 2 shows typical DSC thermographs of the three linear and two branched alkanes here studied. The thermographs of each of the linear alkanes show two distinct melting endotherms. This is indicative of the linear alkanes comprising two distinct crystal populations of differing lamellar thickness. Comparisons

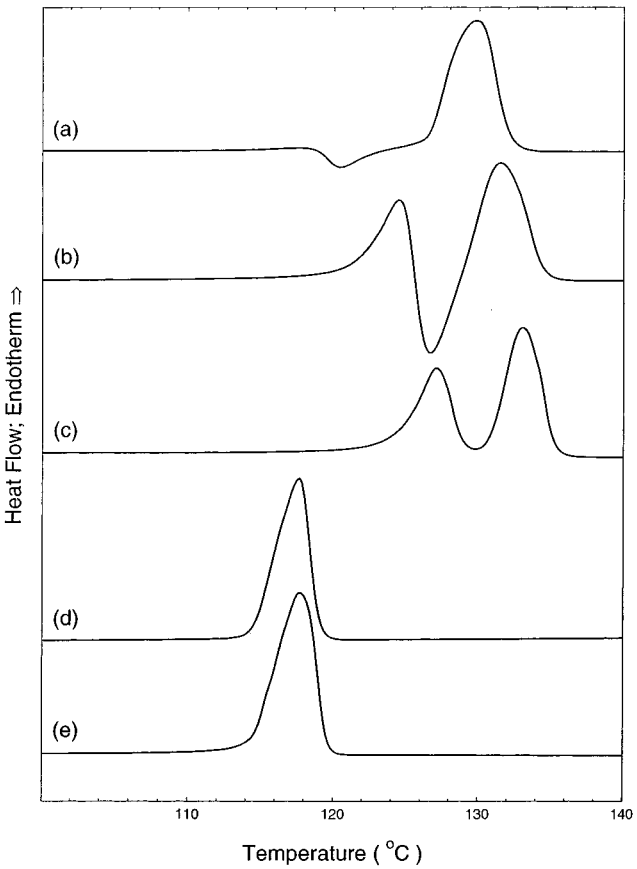


**Figure 2.** DSC thermographs for (a) $C_{198}H_{398}$, (b) $C_{246}H_{494}$, (c) $C_{294}H_{590}$, (d) $C_{96}H_{193}CH(CH_3)C_{94}H_{189}$, and (e) $C_{96}H_{193}CH(C_4H_9)C_{94}H_{189}$.

of the melting onsets (Table 1) with those in the literature[19,27] suggest that these populations are of crystals comprising fully extended (E) chains and exactly once-folded (F1) chains. Another interesting feature of the DSC thermographs of the linear alkanes is the appearance of an exotherm between the two melting endotherms. This is a result of crystal thickening. The crystals comprising folded chains have a significantly lower melting temperature than those comprising extended chains. There is therefore a temperature range where crystals comprising extended chains are stable and those comprising folded chains are not. In this temperature range the folded chain crystals melt and recrystallize as extended chain crystals. The exotherm observed is the crystallization exotherm for these newly formed extended chain crystals. A thickening exotherm is not observed in the thermograph of $C_{294}H_{590}$ (Figure 2c). This does not imply that no thickening occurs; the exotherm is merely hidden through superposition with the melting endotherms.

The thermographs of the branched alkanes show only one melting endotherm. The melting onset here is consistent with crystals comprising once-folded chains with the branches at the fold surface. It has been shown[28] that both methyl and butyl branches can be incorporated into the polyethylene crystal lattice, but in these materials the branches preclude the formation of extended chain crystals because they are all at exactly the same point on the chain. This would produce an intolerable crystal strain at the center of an extended chain crystal. The folded chain crystal is therefore preferred.

**Table 1. Lamellar Thicknesses Determined from DSC Melting Peak Positions, $T_m$, Using Eqs 1 and 2**

| alkane | melting onset (± 0.5 °C) | melting peak (± 1 °C) | lamellar thickness from eq 1 (nm) | lamellar thickness from eq 2 (nm) | "ideal" lamellar thickness (nm) |
|---|---|---|---|---|---|
| $C_{198}H_{398}$ | 118 | 119 | 11 ± 1 | | 10.3 |
| $C_{198}H_{398}$ | 126 | 129 | 17 ± 2 | 18 ± 1 | 20.6 |
| $C_{246}H_{494}$ | 122 | 125 | 13 ± 1 | | 12.7 |
| $C_{246}H_{494}$ | 128 | 132 | 20 ± 1 | 23 ± 2 | 25.6 |
| $C_{294}H_{590}$ | 124 | 128 | 16 ± 1 | | 15.3 |
| $C_{294}H_{590}$ | 130 | 134 | 24 ± 2 | 28 ± 2 | 30.6 |
| $C_{96}H_{193}CH(CH_3)-C_{94}H_{189}$ | 114 | 118 | 10 ± 1 | | 9.8 |
| $C_{96}H_{193}CH(C_4H_9)-C_{94}H_{189}$ | 114 | 118 | 10 ± 1 | | 9.8 |

It is possible to calculate explicitly the lamellar thickness of a crystallite from the position of the melting peak, $T_m$, using eq 1[29]

$$T_m = T_m^0\left(1 - \frac{2\sigma_e}{\Delta h_f l}\right) \quad (1)$$

where $l$ is the lamellar thickness, $T_m^0$ is the equilibrium melting temperature of a crystal of infinitely large $l$, $\Delta h_f$ is the heat of fusion per unit volume of crystal, and $\sigma_e$ is the fold surface interfacial free energy. $T_m^0$ is commonly quoted[29] as 145.8 °C, $\Delta h_f$ as $2.8 \times 10^8$ J m$^{-3}$, and $\sigma_e$ as $(93 \pm 8) \times 10^{-3}$ J m$^{-2}$.

Although interfacial free energy, $\sigma_e$, is a quantity applicable to normal molecular crystals, it is conceptually different in the case of chain-folded crystals. In chain-folded crystals $\sigma_e$ includes contributions from the energy per unit area required to form a chain fold and is independent of molecular weight.[29] A fold requires a number of repeat units in the higher energy gauche conformation, with a corresponding increase in the energy stored in the chain. Clearly, the interpretation of $\sigma_e$ is different for a crystal comprising extended chains, as is manifest in the observed dependence of $\sigma_e$ on molecular weight in the regime of chain-extended crystallization.[30] It is possible to calculate $\sigma_e$ for chains of a given length, but the calculation is cumbersome and the results are unreliable. Instead, the lamellar thickness of a chain-extended crystallite with disordered end sequences can be calculated from eq 2[31]

$$\frac{1}{T_m} - \frac{1}{T_m^0} = \left(\frac{R}{\Delta H_u}\right)\left\{\frac{1}{x} + \frac{1}{x - l + 1}\right\} \quad (2)$$

where $x$ is the number of units in a chain, $l$ is the length of the crystallite, $\Delta H_u$ is the enthalpy of fusion per repeat unit, equal to 4.10 kJ/mol,[30] and $R$ is the universal gas constant.

The results of the lamellar thickness calculations for each of the melting peaks are shown in Table 1. Equation 1 has been used for all peaks and eq 2 only for those crystals assigned through the literature to comprise extended chains. The lamellar thicknesses labeled "ideal" are those calculated from purely geometrical considerations using a bond angle of 109.5° and a bond length of 1.54 Å and assuming 100% chain participation in the crystal and a tilt angle[32] of 35°.

The lamellar thicknesses determined from eq 1 agree well with the ideal thicknesses in the case of chain-folded crystals. This demonstrates that those peaks were correctly assigned to crystals comprising once-folded chains. The agreement is not as good in the case of extended chain crystals, as would be expected, since the value of $\sigma_e$ used is not necessarily applicable to crystals comprising extended chains. Equation 2, however, shows good agreement with the ideal value,

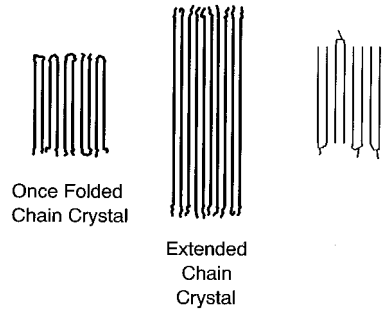


**Figure 3.** Schematic representation of the observed crystalline morphologies: (a) linear, extended chain crystals; (b) linear, once-folded chain crystals; (c) branched, once-folded chain crystals.

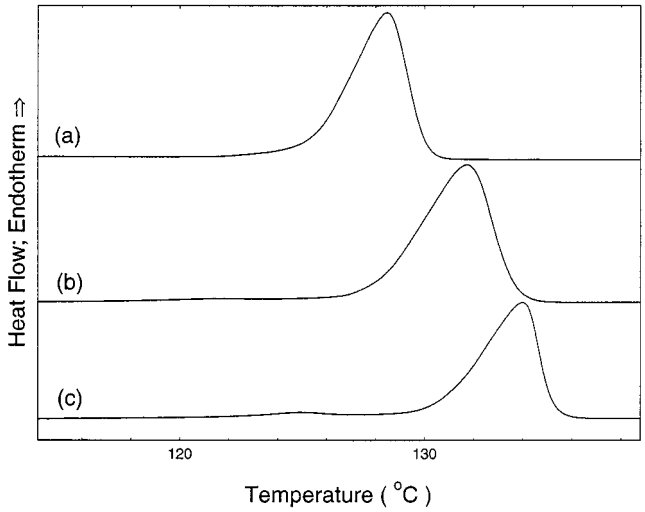


**Figure 4.** DSC thermographs of annealed linear alkanes: (a) $C_{198}H_{398}$, (b) $C_{246}H_{494}$, (c) $C_{294}H_{590}$.

demonstrating that these melting peaks are correctly assigned to extended chain crystals. Any discrepancies are most likely due to the assumption of 100% chain participation. The crystalline morphologies observed are depicted schematically in Figure 3.

**(ii) Preparation of Extended Chain Crystals.** The distinct melting temperatures of the populations of E and F1 crystals allow the morphology produced to be controlled through careful control of the crystallization conditions. For example, annealing a linear alkane at a temperature above the melting temperature of the F1 crystals but below that of the E crystals should result in the production of a sample that exclusively comprises E crystals. This strategy was here employed to produce bulk samples for NMR study which exclusively comprised extended chains crystals. Figure 4 shows the DSC thermographs of the so-prepared linear alkanes. The ideal annealing times and temperatures found are shown in Table 2. As a result of their monodispersity, the alkanes are very highly crystalline, and this crystal-

**Table 2. Optimum Annealing Times and Temperatures of the Linear Alkanes, with Their Crystallinities before and after Annealing As Measured by DSC**

| alkane | annealing temp (°C) | annealing time (min) | crystallinity (±2%) (pre-annealing) | crystallinity (±2%) (post-annealing) |
|---|---|---|---|---|
| $C_{198}H_{398}$ | 119 | 5 | 92 | 99 |
| $C_{246}H_{494}$ | 124 | 5 | 90 | 95 |
| $C_{294}H_{590}$ | 125 | 30 | 89 | 98 |

linity increases with annealing, as would be expected. Postannealing, the thermographs of $C_{198}H_{398}$ and of $C_{246}H_{494}$ show only the endotherm corresponding to E crystals. This demonstrates that these samples comprised exclusively E crystals. In $C_{294}H_{590}$, although the endotherm corresponding to E crystals is much the larger, indicating that the vast majority of crystals formed comprised extended chains, the F1 endotherm is still clearly visible. Ideally, there should be no F1 material present, but, despite the use of a wide range of annealing times, temperatures, and cooling rates, this was not achieved. It is most likely that the F1 crystals formed as the sample was cooled from the annealing temperature.[10] The annealing procedures outlined in Table 2 were used to provide bulk samples for NMR study which comprised exclusively, or almost exclusively, extended chain crystals.

**(iii) Preparation of Folded Chain Crystals.** Crystals comprising folded chains are more likely to be formed the greater the supercooling.[33] Supercooling is defined as $T_m - T_c$, where $T_m$ is the melting temperature and $T_c$ the crystallization temperature. Although the extended chain crystal is the crystal of maximum stability, the probability of chains extending themselves fully in primary nucleation is low at large supercoolings. Chain-folded fluctuations which involve lower free energy barriers are preferred. Even if an extended chain substrate is available, the folded chain crystal growth is still greater due to the large number of possible folded molecular conformations and the large number of possible attachment positions along the extended chain sites.

Accordingly, to prepare bulk samples of alkane exclusively comprising F1 crystals, the samples were quenched to a large supercooling for crystallization. This was carried out for each of the linear alkanes. It was assumed that the branched alkane crystals already exclusively comprised once-folded chains. The alkanes were placed inside DSC pans and heated to 150 °C on a digitally controlled hot plate. When melted, the samples were plunged into liquid nitrogen where they were held submerged for 2 min. Subsequent DSC scans show that at least some F1 crystal had been produced by this method for each of the linear alkanes. However, since the alkane crystals thicken during the DSC experiment (Figure 2), it was impossible to tell from the thermographs whether they had exclusively contained F1 crystals. The folding habit was therefore investigated using X-ray scattering.

SAXS patterns were recorded at room temperature for alkane samples prepared as described above either to comprise exclusively F1 crystals or exclusively E crystals (Figure 5a−c). In each of the scattering patterns only one set of peaks is visible, suggesting that one lamellar thickness was predominant in each case. The position of the peaks in the quenched and annealed samples of the same alkanes is distinctly different in all cases. In the analysis of the patterns a stacked

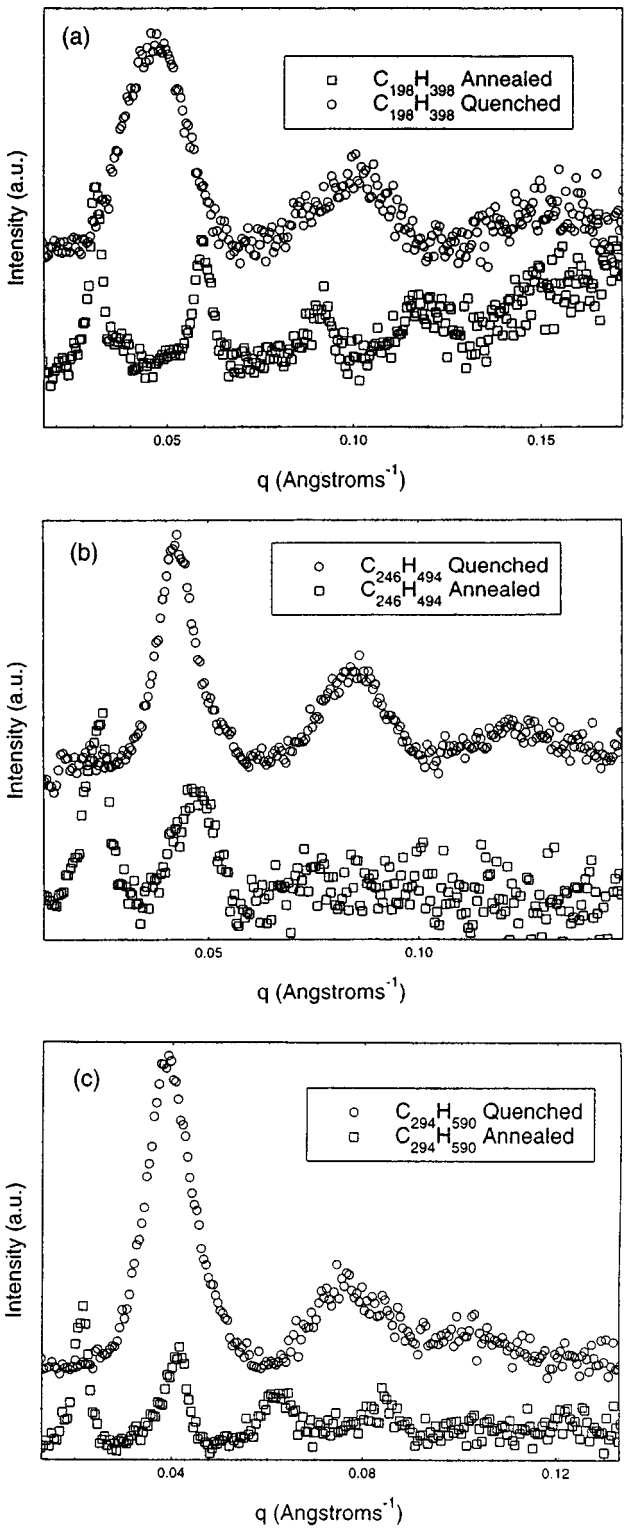


**Figure 5.** SAXS patterns recorded at room temperature for linear alkane samples either quenched to comprise exclusively F1 crystals or annealed to comprise exclusively E crystals: (a) $C_{198}H_{398}$, (b) $C_{246}H_{494}$, (c) $C_{294}H_{590}$.

lamellar morphology was assumed. The long spacings, $d$, were calculated from the peak positions using

$$q = \frac{2\pi}{d} \tag{3}$$

The results are shown in Table 3. The long spacings of the annealed alkanes show excellent agreement with

**Table 3. Crystallinities of the Various Alkanes Measured by DSC, NMR, and SAXS and Their SAXS Long Spacing[a]**

| alkane and preparation | SAXS crystallinity[b] (±4%) | DSC crystallinity (±2%) | NMR crystallinity[c] (±2%) | long spacing (nm) | lamellar thickness (nm) | ideal lamellar thickness (nm) |
|---|---|---|---|---|---|---|
| $C_{198}H_{398}$ (quenched) | 75 | | 76 | 12.9 ± 0.3 | 9.8 (± 0.3 | 10.3 |
| $C_{198}H_{398}$ (annealed) | 87 | 99 | 98 | 20.8 ± 0.4 | 20.4 ± 0.4 | 20.6 |
| $C_{246}H_{494}$ (quenched) | 80 | | 81 | 14.9 ± 0.3 | 12.2 ± 0.4 | 12.7 |
| $C_{246}H_{494}$ (annealed) | 92 | 95 | 98 | 25.8 ± 0.3 | 25.5 ± 0.6 | 25.6 |
| $C_{294}H_{590}$ (quenched) | 76 | | 79 | 16.2 ± 0.2 | 12.8 ± 0.4 | 15.3 |
| $C_{294}H_{590}$ (annealed) | 99 | 98 | 98 | 29.2 ± 0.4 | 28.7 ± 0.7 | 30.6 |
| $C_{96}H_{193}CH(CH_3)-C_{94}H_{189}$ | | 78 | 82 | 10.3 ± 0.2 | 8.5 ± 0.3 | 9.8 |
| $C_{96}H_{193}CH(C_4H_9)-C_{94}H_{189}$ | | 83 | 82 | 10.3 ± 0.2 | 8.5 ± 0.3 | 9.8 |

[a] Lamellar thickness is calculated from the product of SAXS long spacing and NMR crystallinity. [b] Recorded at room temperature. [c] Recorded at 60 °C.

the "ideal" lamellar thickness in each case. This confirms that the annealed samples exclusively comprise E crystals. The similarity between the long spacings and the lamellar thicknesses is also indicative of extremely high crystallinity; the amorphous interlayers are exceptionally thin. The long spacings of the quenched linear and branched alkanes tend to be larger than the "ideal" lamellar thicknesses. These materials are less highly crystalline, and the interlamellar amorphous regions push the crystalline layers apart. Taking this into account, the results are consistent with the quenched linear and branched alkanes exclusively comprising F1 crystals.

**(iv) Folded to Extended Chain Transition Observed by SAXS.** For each of the alkanes a series of SAXS patterns were recorded as the temperature was increased (Figure 6a−e). In each of the linear alkanes (Figure 6a−c) the patterns observed at lower temperature correspond to folded chain crystals. In $C_{294}H_{590}$ (Figure 6c) the lower temperature patterns show only the peaks resulting from once-folded chain crystals which are exactly half the thickness of the crystals comprising extended chains (F1 crystals). In $C_{198}H_{398}$ and $C_{246}H_{494}$ (Figure 6a,b) the lower temperature SAXS patterns are superpositions of the scattering patterns from two distinct crystal populations. These populations are F1 crystals and folded chain crystals whose lamellar thicknesses are a noninteger fraction of the extended chain crystal thickness. These noninteger fraction, or NIF, crystals have a length between that of the E and F1 crystals. Although integer folding is preferred,[18] transient NIF forms are often produced as the result of the much higher attachment probability of noninteger fractions.[33] These transient NIF forms can be frozen in at room temperature if the sample is quenched.[32] Here, to improve the amount of sample placed in the beam, the virgin alkane powders were melted on a hot plate and allowed to cool to room temperature prior to the beginning of each SAXS experiment. This cooling was fast enough to quench in some NIF crystal forms.

Each of the linear alkanes undergoes a lamellar thickening transition at a temperature corresponding to that measured by DSC (Table 1). Following this transition, the patterns for each of the linear alkanes contain peaks corresponding to E crystals. The SAXS patterns of the branched alkanes (Figure 6d,e) show the peaks corresponding to F1 crystals. No evidence of thickening was observed. This is consistent with the DSC measurements and with the assumption that the branches prevent the formation of E crystals.

The alkanes all show increases in intensity as the melting or thickening transitions are approached. This is an effect both of increased scattering contrast and of the partial melting of the crystallites. These factors are related to the scattered intensity for a two-phase structure of volume crystallinity $\varphi$ through[34]

$$4\pi\int_0^\infty q^2 i(q)\,\mathrm{d}q = \varphi(1-\varphi)(\rho_c - \rho_a)^2 \qquad (4)$$

where $\rho_c$ and $\rho_a$ are the electron densities in the crystalline and amorphous phase, respectively, and $i$ is the scattered intensity. As temperature is increased, the expansion of the amorphous phase and the reduction in crystallinity toward 50% both tend to increase the scattered intensity. Crystallinity can be calculated from the ratios of the integrated intensities of the $h$th-order reflection to that of the first order using[34]

$$\frac{(I)_h}{(I)_1} = \frac{\sin^2(h\pi\varphi)}{h^2 \sin^2(\pi\varphi)} \qquad (5)$$

where $I_h$ and $I_1$ are the integrated intensities of the $h$th and first orders, respectively. For $C_{294}H_{590}$ this yields a reduction in crystallinity from 70% to 64% in the temperature range 110−120 °C, which is in good agreement with measurements of the change in crystallinity with temperature made from $^1$H broadline NMR.[35]

**(v) Alkane Crystallinity.** Table 3 shows the results of the crystallinity measurements made on the well-characterized E and F1 crystals with three techniques: SAXS, DSC, and NMR. The results show good agreement, especially when the different physical properties probed by the different techniques are considered. The lamellar thickness has been calculated from the product of the long spacing and the crystallinity as measured by $^1$H NMR. These are the values of lamellar thickness carried on into the following $^{13}$C NMR analysis.

**(vi) WAXS Analysis.** A series of WAXS patterns were recorded for each of the alkanes as the temperature was increased. The patterns were similar for each alkane, and a typical example is shown in Figure 7. The 110 and 200 peaks of orthorhombic polyethylene were observed for each sample. The unit cell showed no distortion in the branched samples, further confirming the branches' exclusion[28] from the F1 crystals. At the thickening transition the scattered intensity passed through a minimum. This is the result of large-scale melting and recrystallization. The thickening transition was observed to cause no change in the unit cell dimensions.

**NMR Results.** $^{13}$C MAS NMR spectra were obtained for each of the alkanes. A typical spectrum is shown in Figure 8. Four distinct peaks are visible: the crystalline

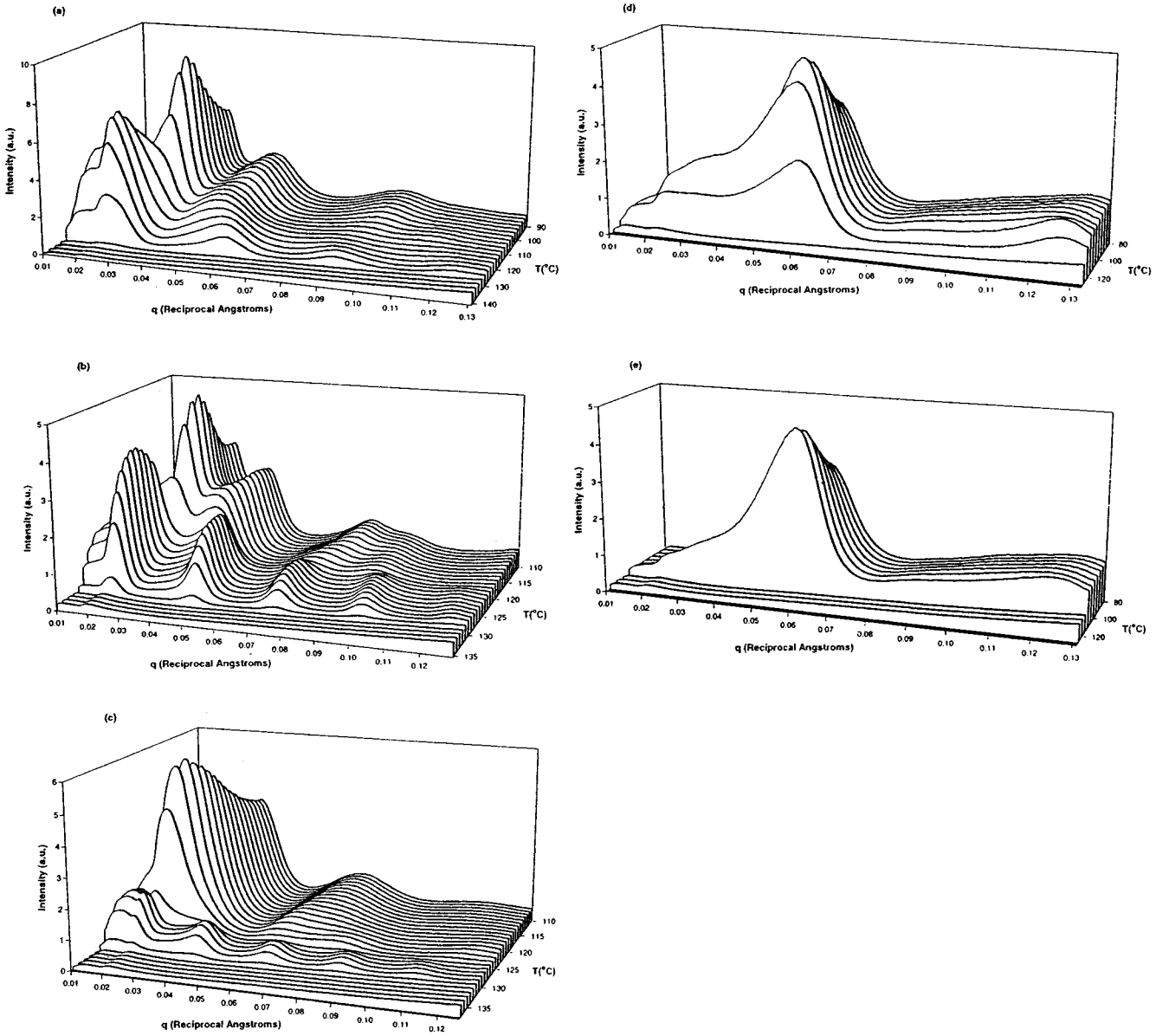


**Figure 6.** Variable temperature SAXS scans for (a) $C_{198}H_{398}$ heated at 5 °C/min, (b) $C_{246}H_{494}$ heated at 1 °C/min, (c) $C_{294}H_{590}$ heated at 1 °C/min, (d) $C_{96}H_{193}CH(CH_3)C_{94}H_{189}$ heated at 5 °C/min, and (e) $C_{96}H_{193}CH(C_4H_9)C_{94}H_{189}$ heated at 5 °C/min. SAXS scans for the linear alkanes show the change from folded to extended chain crystals. Those for the branches alkanes show only folded chain crystals.

peak at 32.5 ppm, the amorphous peak at 31 ppm, the end methyl carbon at 13.5 ppm, and the penultimate carbon at 24 ppm.[36] Figure 9 shows a typical set of spectra taken at various recycle delays, ranging from 2 to 1200 s. It can be seen that the amorphous peak, and those of the end groups, have constant intensity, indicating that they are fully relaxed within 2 s. This is a consequence of the relatively high mobility of the noncrystalline phase leading to a $T_1$ of about 0.5 s.[37] In contrast, the crystalline signal shows an increase in intensity over the whole range of recycle delays. This slow growth in intensity indicates that the crystal phase takes a prolonged time to recover its equilibrium magnetization. It is this recovery which has traditionally been analyzed in terms of a classical $T_1$ relaxation but which we are now attributing predominantly to crystalline chain diffusion.[11−13] A section of chain within the crystal diffuses into the amorphous phase, where it can experience efficient relaxation, and back into the crystal, during the recycle delay. The fractional growth in the intensity of the crystalline peak, $M(t)/M_0$, can be found as[12]

$$\frac{M(t)}{M_0} = \frac{f_c(t)}{1 - f_c(t)} \frac{1 - \chi}{\chi} \tag{6}$$

where $f_c(t)$ is the fraction contributed by the crystalline peak in the $^{13}C$ spectrum at any time and $\chi$ the crystallinty measured from the broadline proton spectrum. We assume in the analysis that for most samples the intrinsic $T_1$ of the crystalline carbons is very long by comparison to the diffusional process.[11,12,38]

**Effect of Crystallinity on Chain Diffusion.** Figure 10 shows the recovery of the crystalline magnetization as a function of the square root of the recycle delay, normalized by the lamellar thickness, for the E and F1 samples of $C_{246}H_{494}$ and $C_{294}H_{590}$. The relaxations of the different alkanes overlap each other, illustrating that the relaxation scales with lamellar thickness in exactly

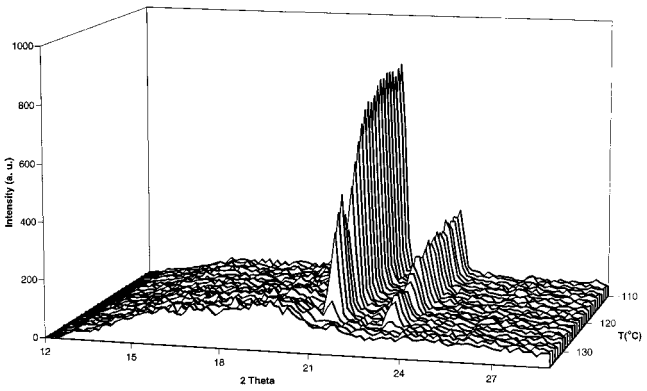


**Figure 7.** A typical variable temperature WAXS pattern for a linear alkane. The pattern shown is for $C_{294}H_{590}$ heated at 1 °C/min. The 110 and 200 peaks of orthorhombic polyethylene are visible.

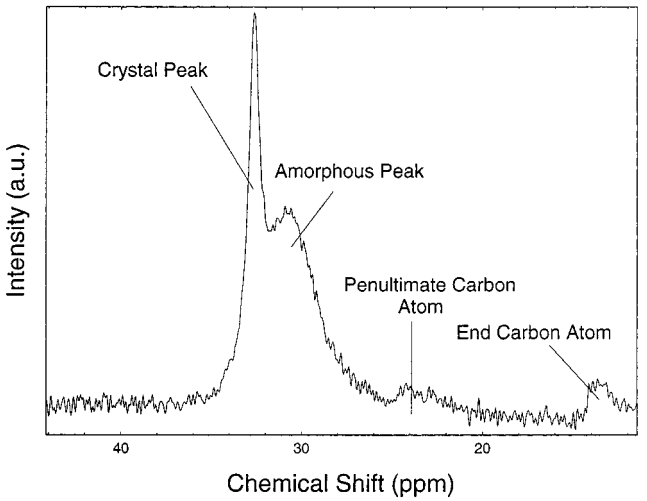


**Figure 8.** A typical alkane $^{13}C$ NMR spectrum. The spectrum shown is for $C_{294}H_{590}$ recorded at 60 °C using a progressive saturation pulse sequence with a recycle delay of 2 s. The peaks are assigned according to ref 36.

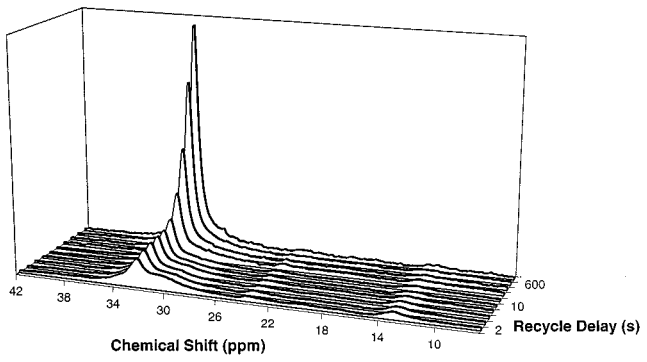


**Figure 9.** $^{13}C$ NMR spectra at various recycle delays between 2 and 1200 s. The enhancement with time of the crystalline resonance, at 32.5 ppm, occurs over several hundred seconds, while the noncrystalline resonances are fully relaxed within 2 s.

the way one would expect for a diffusional process. Distinct differences were observed in the time scales of the relaxations of the samples comprising E and F1 crystals. The extended chain crystals relaxed significantly more slowly than the folded chain crystals for each alkane, and the maximum recovery observed was only about 20% at the longest time studied (1200 s). Initially, this might seem counterintuitive, as a chain

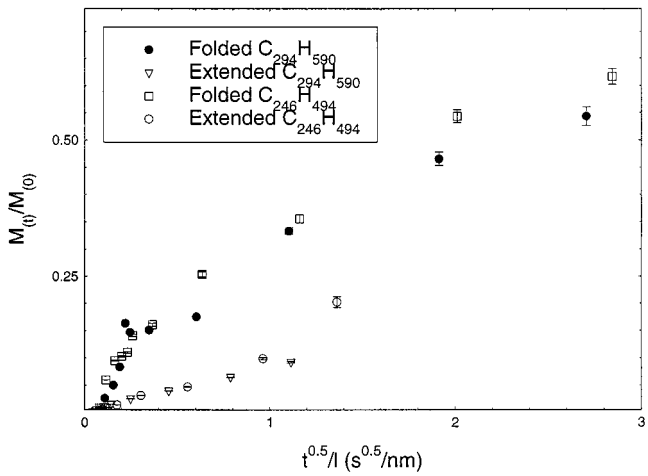


**Figure 10.** Fractional recovery of the crystalline magnetization, against the square root of the recycle delay, normalized by the lamellar thickness, for the E and F1 samples of $C_{246}H_{494}$ and $C_{294}H_{590}$.

fold would be expected to suppress the diffusion process, leading to a slower recovery in the F1 crystals. The explanation proposed here for the observed behavior is that the exceptionally high crystallinity of the extended chain samples causes them to relax extremely slowly. Since the crystallinity of the samples does not change with time, this implies that the vacancy left by a chain stem exiting a lamella will be filled by a chain entering from the interface on the other side. The diffusion rate, then, is determined to some extent by the probability of amorphous cilia entering vacancies in the basal plane, which will be greater for a longer section of amorphous chain. It is therefore not unreasonable to suggest that the transport process should become progressively more difficult as the crystalline fraction increases. Such a trend has recently been observed in $^1H$ NMR $T_1$ relaxations of polyethylene.[39] The exceptionally high crystallinities (~95%) of extended chain $C_{246}H_{494}$ and $C_{294}H_{590}$ produce slower diffusion than any obstacle to chain diffusion presented by the addition of chain folds, resulting in the slower recovery of the E crystals. The F1 crystals have significantly lower crystallinities of about 80%, and we consider the constraints to diffusion to be largely due to the chain folds, as will be discussed later.

**Crystal Morphology of $C_{198}H_{398}$ and Effect of Chain Folding.** Figure 11 shows the relaxations of all the quenched linear alkanes. The relaxation of $C_{198}H_{398}$ differs significantly from that of the others. To explain this quicker relaxation, it is necessary to consider the crystal morphology formed. $C_{198}H_{398}$ is the shortest alkane investigated and therefore the most difficult with which to prepare samples exclusively comprising F1 crystals. The shortest chain in which folding has been observed[17] is $C_{150}H_{302}$. Although SAXS measurements demonstrated that the lamellar thickness corresponded to F1 crystals, this does not necessarily show that the crystals are of the desired type; crystals comprising a mixture of F1 and E chains could still have a lamellar thickness consistent with F1 crystals (Figure 12). The likelihood of the formation of this type of morphology is increased for a quenched sample. X-ray studies of similar linear alkanes have shown that it is possible for some chains to be folded and fully crystalline while others are only half crystallized in the initial stages of crystallization.[32] The partially crystallized chains are

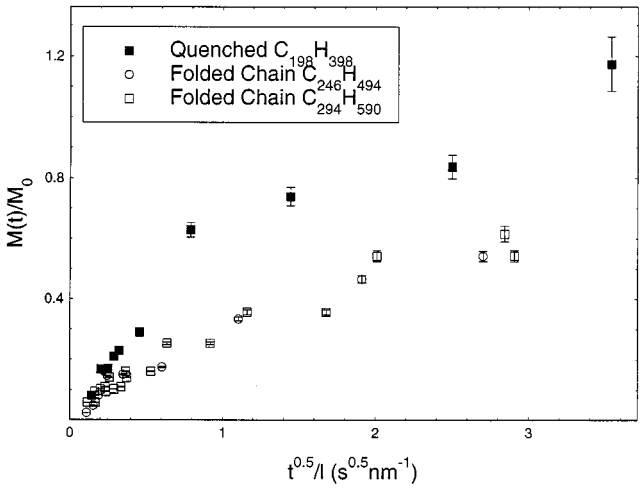


**Figure 11.** $^{13}C$ relaxation data for the quenched, linear alkanes. $C_{198}H_{398}$ relaxes significantly more quickly than the other quenched alkanes.

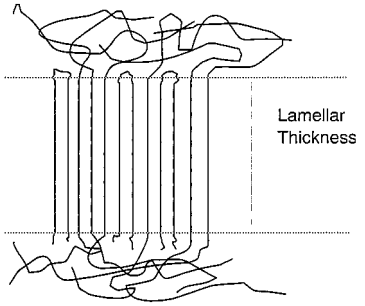


**Figure 12.** Schematic diagram of the crystalline morphology of quenched $C_{198}H_{398}$. Although the crystal comprises a mixture of folded and extended chains, the lamellar thickness is indistinguishable from that of an F1 crystal.

not folded, and each traverses the lamella once (Figure 12). By rapid melt quenching it is possible to freeze this crystal form at room temperature.

If it is assumed that chain folds do represent some form of obstacle to the diffusion process, then the formation of the type of crystals shown in Figure 12 explains the faster recovery of the quenched $C_{198}H_{398}$. Since we are assuming that this sample did not exclusively comprise F1 crystals, but rather a mixture of folded and partially crystallized extended chains, perhaps even a majority of extended chains, there were fewer restraints to chain diffusion than in the true F1 samples, leading to the observed rapid recovery of magnetization. $C_{198}H_{398}$ also has a slightly lower crystallinity than the other two quenched alkanes, which is consistent with the morphology proposed. These levels of crystallinity would not suppress the diffusion of the partially crystallized extended chains in the way suggested for the very high crystallinity E chains discussed earlier. Furthermore, the magnetization in this sample recovers to 100%. Considering purely diffusion, this implies that an entire chain stem can escape from the lamella on a time scale of 1200 s. This is unlikely, especially for the fraction of the sample comprising folded chains, where the amorphous part of the chain represented by the loose chain fold would not be able to recrystallize by entering an adjacent lamella. An alternative explanation for the recovery approaching 100% at long times is a contribution from the intrinsic $T_1$ of the crystal. This may be relatively short due to the disordered fold surface increasing the lattice spacing near the edge of the lamellae and is discussed in more detail below.

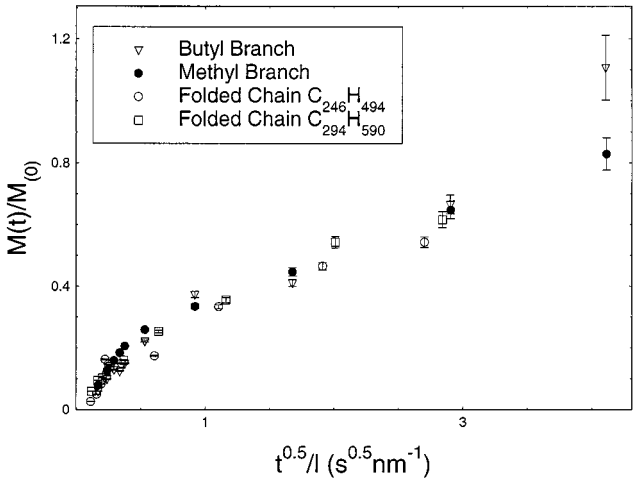


**Figure 13.** $^{13}C$ relaxation data for F1 crystals of linear and branched alkanes. There is no significant difference between the relaxation rates of the linear and branched alkanes.

**Effect of Branching.** Figure 13 shows the recovery of magnetization for the branched alkane samples, $C_{96}H_{193}CH(CH_3)-C_{94}H_{189}$ and $C_{96}H_{193}CH(C_4H_9)-C_{94}H_{189}$, referred to as the methyl- and butyl-branched samples, respectively. It has been demonstrated that these materials form F1 crystals with the branches at the fold surface. The recoveries are the same for each of the branched samples. This is unsurprising since we know that, in these materials, branches of differing lengths are equally excluded from the crystals. Figure 13 also shows the recoveries of the F1 linear crystals. Remarkably, there is no significant difference between the recoveries of the F1 linear and the F1 branched samples. This result leads to the surprising conclusion that the addition of a branch at the fold surface does not make a significant difference to the constraint posed by the fold itself. This will be discussed further in the following section. It is also worth noting that the similarity of the relaxations of the F1 branched and linear samples supports the assumption that quenched $C_{246}H_{494}$ and $C_{294}H_{590}$ form true F1 crystals rather than the mixed crystals discussed in the preceding section. We again see recoveries approaching 100% for the branched samples, similar to $C_{198}H_{398}$. Since all the chains in these samples are once-folded, this again suggests a significant $T_1$ contribution to the relaxation.

**Modeling the Recovery of Magnetization as a Conventional $T_1$ Process**. Before we provide a full analysis of the magnetization recovery based upon chain diffusion, it is necessary to consider an interpretation based upon multicomponent $T_1$'s. A number of approaches can be adopted; the data can be fitted to two components after Cheng et al.,[40] whereby the longer component is associated with the crystalline core and the shorter one predominantly, but perhaps not exclusively, with the interface. Second, a three-component crystalline $T_1$, as proposed by Kitamaru et al.,[41] where all of these components are assigned to the crystalline phase, as the interfacial component is considered to contribute to the peak at 31.1 ppm. Each of these methods provides a perfectly good fit to the data, and Table 4 shows the results from the two-parameter fit as an illustration. Here, the lamellar thicknesses are taken from Table 3, and the interfacial fraction and the

**Table 4. Lamellar Thicknesses and Parameters Obtained from $T_1$ Fitting Using the Method of Cheng et al.[40]**

| material | lamellar thickness (nm) | interfacial fraction | interfacial $T_1$ (s) | crystalline $T_1$ (s) |
|---|---|---|---|---|
| quenched C198 | 9.8 | 0.18 | 3.73 | 125 |
| quenched C246 | 12.2 | 0.16 | 5.13 | 1019 |
| quenched C294 | 12.8 | 0.17 | 10.5 | 1589 |
| annealed C246 | 25.5 | 0.02 | 17.2 | 6500 |
| annealed C294 | 28.7 | 0.03 | 21.5 | 15500 |
| methyl branch | 8.5 | 0.25 | 6.9 | 729 |
| butyl branch | 8.5 | 0.20 | 6.0 | 528 |

two $T_1$ values are obtained from the biexponential fitting. One must exercise caution in assigning the parameters exclusively to interface and crystal core, as variations in $T_1$ are probably continuous rather than discrete; however, the following observations can be made. The calculated interfacial fraction is much lower in the annealed samples, consistent with their higher crystallinity, and is highest in the branched samples, where the branches are clustered at the fold surfaces. The interfacial $T_1$ is also highest in the annealed samples, which might be expected on the grounds of restricted mobility. The variation in the interfacial $T_1$'s of the other samples is not easy to interpret. We now consider the variations in the magnitude of the $T_1$ values of the crystalline core. The annealed samples have the same crystallinity and the same morphology, and yet the $T_1$ of $C_{294}H_{590}$ is more than twice as long as for $C_{246}H_{494}$. There is also a big difference between quenched and annealed samples and an order of magnitude difference between quenched $C_{198}H_{398}$ and the other quenched samples. The intrinsic $T_1$ within the crystal is considered to be due mainly to small-amplitude torsional oscillations,[42] and so any interpretation of these differences based upon a conventional $T_1$ process must explain why torsional oscillations vary with morphology. It might be argued that quenching, annealing, and different lamellar thicknesses all produce variations in the lattice packing (due to distance from the fold surfaces and changing looseness/tightness of the folds) and therefore variations in the amplitude of the torsional oscillations, and this is indeed consistent with the observed changes in $T_1$ for quenched and annealed $C_{246}$ $H_{494}$ and $C_{294}$ $H_{590}$. The branched samples, where the branch would be expected to cause a greater disruption to the lattice packing, also follow this trend, with the more bulky butyl branch leading to a shorter $T_1$ than the methyl branch. However, the $T_1$'s of these samples are far higher than for quenched $C_{198}H_{398}$, which is counterintuitive. Furthermore, there is no evidence from any of the other techniques (DSC, WAXS, SAXS, broadline NMR) for a change in the lattice spacings. It is worthwhile mentioning here a previous study by one of the authors[12] on radiation-cross-linked polyethylene. When the longitudinal relaxation was interpreted via a $T_1$ analysis as above, it was found that the long $T_1$ *increased* with irradiation dose and gel fraction. Since the effect of cross-links at the fold surfaces would be to increase the lattice spacing, it would be expected, from the foregoing arguments, that $T_1$ should decrease. The results were, however, entirely consistent with a chain diffusion analysis, with the diffusion coefficients decreasing by a factor of 2 from the un-cross-linked sample to one containing 87% gel fraction. We therefore consider that a more convincing explanation for the recovery of longitudinal magnetization is that of chain diffusion, especially at short times. However, the intrinsic $T_1$ of the crystalline phase will contribute to a greater or lesser extent, especially at longer times. We consider this to be the reason for the recovery to approach 100% in some cases, for example the quenched $C_{198}H_{398}$ (Figure 11) and the branched samples (Figure 13), where the crystalline $T_1$ may be relatively short, for the reasons mentioned above. The alternative explanation for the 100% recovery would be that the entire chain escapes from the lamella via a diffusional process, which is perhaps unrealistic on thermodynamic grounds.

**Modeling the Recovery of Magnetization as a Physical Transport Process**. Previous workers[12] have interpreted $^{13}C$ relaxation data via an analysis based upon classical diffusion.[43] They considered the lamella to be a slab of thickness $2l$ with magnetization diffusing in from infinite wells in the interfacial/amorphous regions at either end. The initial concentration of magnetization within the lamella was zero and would grow with time as

$$\frac{M(t)}{M_0} = 1 - \sum_{n=0}^{\infty} 2C_n \exp\left[-\frac{Dt}{C_n l^2}\right] \qquad (7)$$

where $C_n = 4/[(2n + 1)^2\pi^2]$ and $D$ is the diffusion coefficient. A more illustrative description of crystalline chain diffusion can be developed through analogy with reptation. An alkane chain within a lamellar crystal undergoes a one-dimensional random walk along its own axis. Each time a carbon nucleus moves out of the crystal it relaxes its magnetization via a classical $T_1$ mechanism. The fraction of crystalline magnetization that has relaxed is, therefore, the fraction of the chain that has left the crystal. This situation is exactly analogous to that of a reptating chain in a fixed network.[44] In the tube model for reptation the situation is reduced to a one-dimensional diffusion process. Only the diffusion of the primitive chain, a coarse grain representation of the real chain, is considered, and it is restricted to move only back and forth along its axis. The fraction of the chain remaining in the tube and therefore unrelaxed, $\psi$, at some time, $t$, is given by

$$\psi = \sum_{p;\text{odd}} \frac{8}{p^2\pi^2} \exp\left[-\frac{p^2 t}{\tau_D}\right] \qquad (8)$$

where $\tau_D$ is the reptation time, the time taken for the primitive chain to disengage from the tube in which it was confined at $t = 0$. The $^{13}C$ relaxation can therefore be modeled as

$$\frac{M(t)}{M_0} = 1 - \sum_{p;\text{odd}} \frac{8}{p^2\pi^2} \exp\left[-\frac{p^2 t}{\tau_D}\right] \qquad (9)$$

It should be noted that eqs 7 and 9 are in fact exactly equivalent, although the reptation analogy provides a better insight into the crystal chain diffusion process. Figure 14 shows fits of eq 9 to relaxation data from F1 and E $C_{246}H_{494}$ and from quenched $C_{198}H_{398}$. The only fitting parameter is the reptation time, $\tau_D$. From Figure 14 it can be seen that the reptation model satisfactorily represents the relaxations where the crystals comprise exclusively, or almost exclusively, E chains. This is further evidence for the morphology of quenched $C_{198}H_{398}$ discussed above. The reptation model provides a much

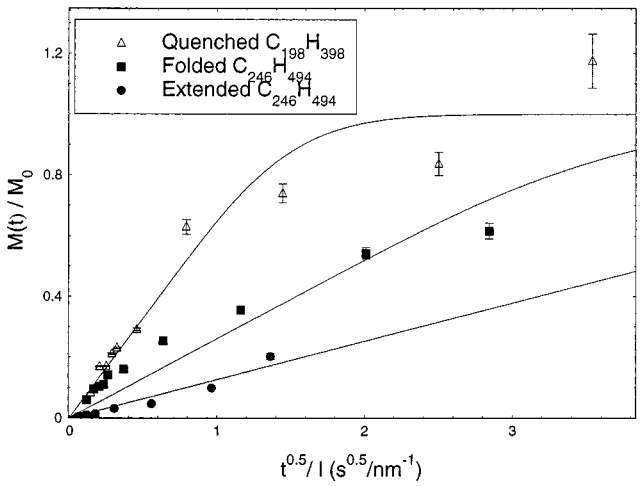


**Figure 14.** $^{13}C$ relaxation data for F1 and E $C_{246}H_{494}$ and for quenched $C_{198}H_{398}$. The lines through the data are fits to a one-dimensional diffusion equation with a single reptation time, eq 9.

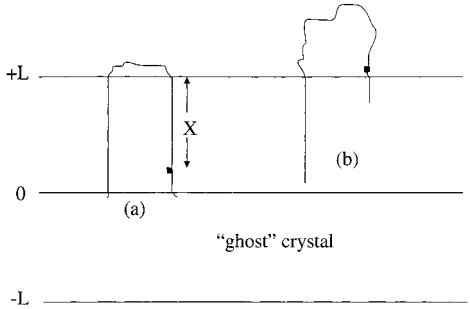


**Figure 15.** Schematic representation of diffusion through fluctuation of fold length. A section of the chain (*X*) close to 0 cannot diffuse into the amorphous phase at the nearest edge (0). Instead, it must diffuse out at $+L$ through fluctuation of the fold length.

less satisfactory representation of the relaxations in the case of F1 crystals. This is because eq 9 does not take into account the effects of any constraints to the diffusion process, such as chain folds.

The relaxation rates of the F1 linear and branched samples are the same (Figure 13). It does not seem possible that a branched alkane could diffuse through a crystal, dragging a group as large as a butyl group with it, distorting each unit cell it comes to. It is certainly extremely unlikely that dragging a branch through a crystal would not affect the rate of diffusion. Therefore, within the context of a diffusional model for the relaxation of magnetization, the alkanes must relax by a motional process which does not require the transport of branches through the crystal. Rather than sliding around the chain fold, which would require drawing a branch into a crystal, branched alkanes can diffuse out of the crystal by partially withdrawing one or both stems from the crystal, fluctuating the length of the chain fold (Figure 15). Such motion allows exchange of material between the crystalline and amorphous phases without requiring that the branch be drawn into the crystal. A similar chain dynamic has been recently proposed in a study concerning crystallization and subsequent structural rearrangement in these branched alkanes.[32] If sliding around a tight chain fold in F1 linear alkanes was similarly prohibitive, the preferred mechanism being the fold length fluctuations described above, then the addition of a branch at the

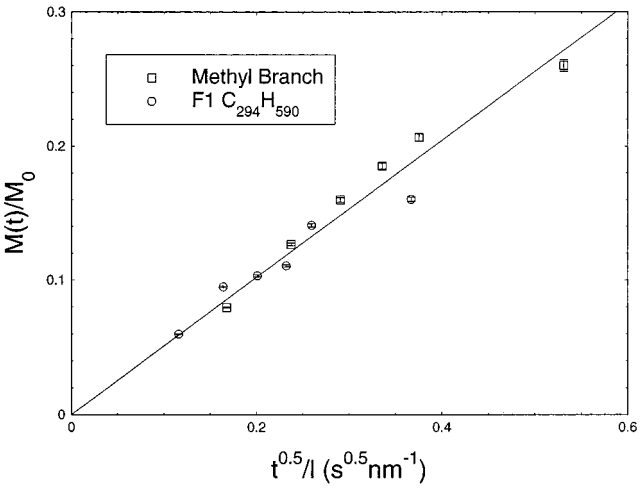


**Figure 16.** $^{13}C$ relaxation data for the initial stages of the relaxations of F1 $C_{294}H_{590}$ and $C_{96}H_{193}CH(CH_3)C_{94}H_{189}$. The line through the data is a fit to eq 9.

**Table 5. Diffusion Coefficents from Fits of Eq 9 to the Initial Stages ($\tau_{rd} \leq 30$ s) of the Relaxation and from Fits over the Full Range of the Relaxation**

| sample | *D:* initial stages ($nm^2\ s^{-1}$) | *D:* full range ($nm^2\ s^{-1}$) |
|---|---|---|
| folded $C_{246}H_{494}$ | 0.047 | 0.013 |
| folded $C_{294}H_{590}$ | 0.049 | 0.011 |
| methyl branch | 0.053 | 0.013 |
| butyl branch | 0.033 | 0.016 |
| quenched $C_{198}H_{398}$ | 0.092 | 0.085 |
| extended $C_{246}H_{494}$ | 0.0013 | 0.0018 |
| extended $C_{294}H_{590}$ | 0.0013 | 0.00093 |

fold surface would not represent an additional constraint to the diffusion process. This would lead to the relaxation time in both the F1 linear and F1 branched samples being the same, as is observed experimentally.

Figure 16 shows eq 9 fitted to the initial stages of the relaxation in the linear and branched F1 crystals. In this range, the reptation model provides a quite acceptable representation of the data. This is a result of the reduced effect of constraints in this region. At short times the longitudinal relaxation is dominated by the free diffusion of chains. Initially, a chain stem sliding out of a crystal undergoes diffusion similar to that experienced by an extended chain. Constraints become more significant as the diffusion continues. Similar effects have been noticed for polyethylene crystals with cross-links added at the fold surface.[12] This can also be thought of in terms of fluctuating lengths of chain folds. If a fold is loose, it presents little or no constraint to the diffusion process, each of the stems being able to diffuse independently, like extended chains. The initial relaxation is due to the diffusion of this unconstrained, loose fold material. The remaining part of the relaxation is due to diffusion of tight, constrained chain folds and proceeds more slowly. This can be further illustrated by comparing the diffusion coefficients obtained from the initial stages of the relaxation ($\tau_{rd} \leq 30$ s) with those obtained over the full range of recycle delay (Table 5). Diffusion coefficients can be easily obtained from eq 9 using

$$\tau_D = \frac{l^2}{\pi D} \tag{10}$$

where *l* is the lamellar thickness. In the case of the F1,

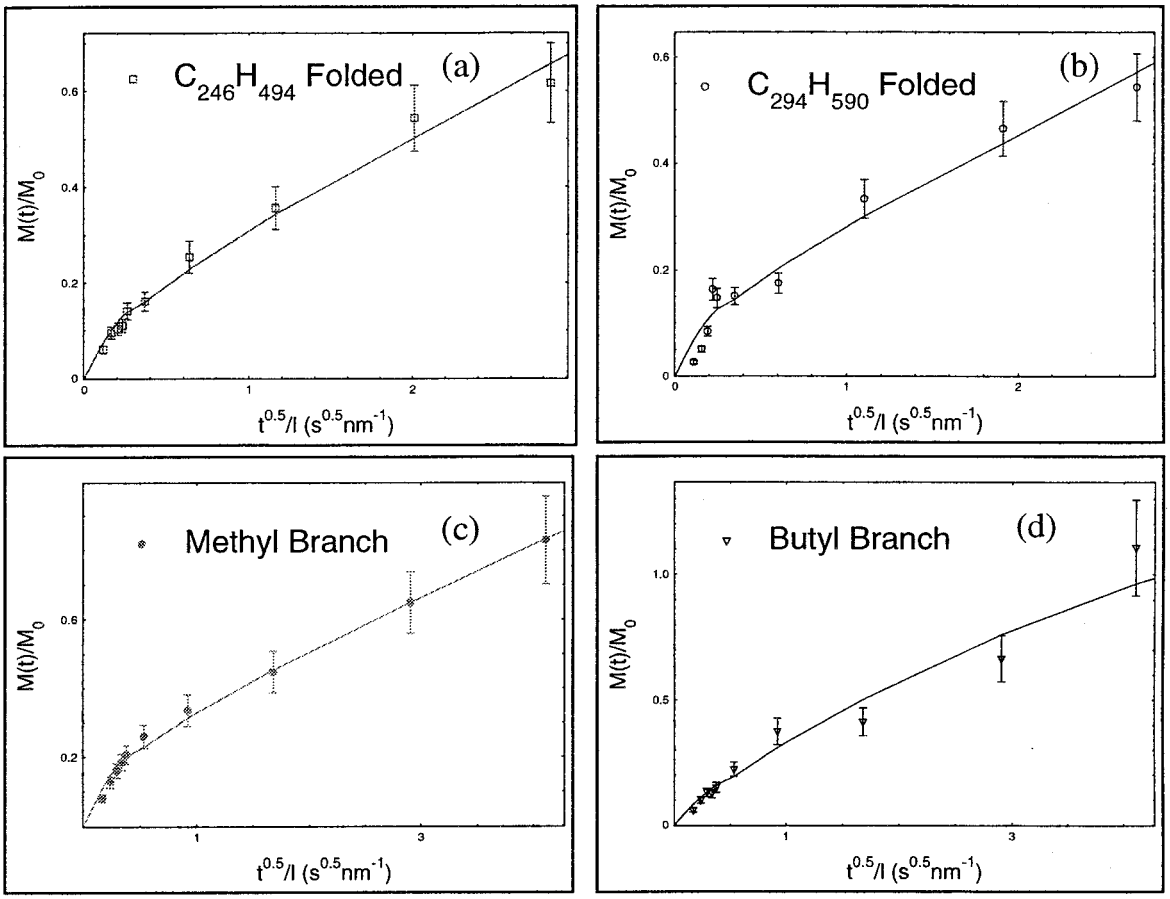


**Figure 17.** $^{13}C$ relaxation data for F1 crystals of (a) $C_{246}H_{494}$, (b) $C_{294}H_{590}$, (c) $C_{96}H_{193}CH(CH_3)C_{94}H_{189}$, and (d) $C_{96}H_{193}CH(C_4H_9)$-$C_{94}H_{189}$. The lines through the data are fits to a dual reptation time one-dimensional diffusion equation, eq 11.

constrained crystals there is a large difference between the diffusion coefficients obtained over the full range of data and those obtained from the short time data. This is consistent with constraints becoming increasingly more significant at longer times. With the E chain samples the diffusion coefficients are very similar over the two ranges. This reflects the satisfactory representation of these data by eq 9. E crystals have no constraints to suppress the diffusion at longer times. In the case of the annealed samples, the exceptionally high crystallinity clearly suppresses diffusion even on very short time scales.

The existence of two distinct regimes of diffusion, constrained and unconstrained, suggests that the $^{13}C$ relaxation of the F1 samples might be better described by a modified version of eq 9 which includes two different reptation times, $\tau_{D1}$ and $\tau_{D2}$. The shorter reptation time, $\tau_{D1}$, corresponding to the larger diffusion coefficient, would dominate in the initial stages of the relaxation. The larger reptation time, $\tau_{D2}$, corresponding to the lower diffusion coefficient, would dominate in the later stages of the relaxation. Such a dual reptation time diffusion model is

$$\frac{M(t)}{M_0} = \exp\left(-\frac{t}{\tau_L}\right)\left[1 - \sum_{p;\text{odd}}^{\infty} \frac{8}{p^2\pi^2} \exp\left(-\frac{p^2 t}{\tau_{D1}}\right)\right] + \left\{1 - \exp\left(-\frac{t}{\tau_L}\right)\right\}\left[1 - \sum_{p;\text{odd}}^{\infty} \frac{8}{p^2\pi^2} \exp\left(-\frac{p^2 t}{\tau_{D2}}\right)\right] \quad (11)$$

where $\tau_L$ is a parameter which indicates the time scale over which diffusion characterized by $\tau_{D1}$ becomes negligible and that characterized by $\tau_{D2}$ dominant. This can be thought of as the time scale over which chains begin to "feel" their constraints and no longer diffuse freely. This parameter is not optimized in the fitting procedure but is set to 30 s by inspection of the data (Figure 13). There are therefore just two adjustable parameters, $\tau_{D1}$ and $\tau_{D2}$. Fits of eq 11 to the F1 crystals' relaxations are shown in Figure 17a−d. Equation 11 provides an excellent representation of the data, performing much better than the single reptation time equation. We have, however, increased the number of fitting parameters, and it is important to carefully consider the values of $\tau_{D1}$ and $\tau_{D2}$ obtained to test the validity of a dual reptation time model.

**Table 6. Diffusion Coefficients Obtained from Fits to the Dual Reptation Model, Eq 11**

| sample | $D_1$ (nm$^2$ s$^{-1}$) | $D_2$ (nm$^2$ s$^{-1}$) |
|---|---|---|
| $C_{246}H_{494}$ folded | 0.089 | 0.0069 |
| $C_{294}H_{590}$ folded | 0.081 | 0.0056 |
| methyl branch | 0.093 | 0.0047 |
| butyl branch | 0.050 | 0.0093 |
| mean | 0.078 ± 0.01 | 0.0067 ± 0.001 |

Diffusion coefficients calculated from $\tau_{D1}$ and $\tau_{D2}$, $D_1$ and $D_2$, respectively, are displayed in Table 6. $D_1$ is the diffusion coefficient corresponding to the initial, unconstrained diffusion of chains. This can be compared to the diffusion coefficient obtained from quenched $C_{198}H_{398}$, an alkane of comparable crystallinity which has been demonstrated to comprise, to a large extent, extended chain crystals. The mean $D_1$ of the F1 samples is 0.078 ± 0.01 nm$^2$ s$^{-1}$. The diffusion coefficient for the largely

freely diffusing $C_{198}H_{398}$ is 0.085 nm$^2$ s$^{-1}$ (Table 5). The agreement between these two diffusion coefficients is a very strong piece of evidence to support the proposal that the initial part of the diffusion is the diffusion of free chains before any constraints are felt.

The $D_2$ values, corresponding to constrained diffusion, are considerably smaller than the $D_1$ values, as would be expected. This is consistent with the suppression of diffusion by constraints in the later stages of the relaxation, as is the observed reduction in the diffusion coefficient of approximately 1 order of magnitude. At this point, we should address the fact that recovery at longer times is also influenced by $T_1$ relaxation, especially for $C_{198}H_{398}$ quenched and the branched samples, and this will affect the value of $D_2$. Since the diffusion model involves a summation of exponentials (eqs 9 and 11), the $T_1$ contribution will merely be included as a term in this sum. In a simple view of diffusion through fold length fluctuations, the chain folds act to restrict the diffusion in two ways. First, loosening or tightening a chain fold requires both chain stems to move in or out of a lamella, respectively. One stem moving out while the other moved in would lead to sliding around the fold. In the freely diffusing case ((b) in Figure 15) this sliding is allowed, but where folding is tight and constraints are felt ((a) in Figure 15) it is not. Progressing from (a) to (b) in Figure 15 would require both stems to move out of the crystal. This does not imply that the two stems have to jump at the same time or that the stems must withdraw from the crystal at the same rate. It is the direction in which the stems can move which is restricted. Requiring cooperative motion of the chain stems in this sense would result in a reduction in the diffusion coefficient by a factor of 2.

The inability of the chain to slide around the chain fold also restricts the diffusion in a second way. Material close to the edge of the lamella at the opposite side from the fold cannot diffuse into the amorphous phase at the nearest edge (Figure 15). Instead, this material must diffuse out at the edge of the crystal where the fold is. This condition that the chain section must diffuse out at the same edge of the crystal is analogous to the situation of an extended chain crystal of twice the lamellar thickness. This effect would reduce the diffusion coefficient by a further factor of 4. The overall effect of constraints upon the fold length fluctuation diffusion mechanism would then be predicted to be approximately the 1 order of magnitude ($2 \times 4$) observed experimentally. This strongly supports both the proposed diffusion mechanism and the dual reptation time equation.

It is also instructive to compare the diffusion coefficient within the crystal to the diffusion coefficient of the same length of chain within the melt at the same temperature. The self-diffusion coefficient of the center of mass of a chain in the melt, $D_G$, is given by[44] eq 12.

$$D_G = \frac{b^2}{3\pi^2\tau N} \tag{12}$$

where $N$ is the number of Rouse units in the chain, $b$ the length of the fundamental Rouse unit, and $\tau$ its relaxation time. NMR has been used[45] to determine $\tau$ at 149 °C as $1.5 \times 10^{-8}$ s. Applying a WLF shift to 60 °C, the same temperature as the crystalline diffusion, gives $\tau$ at 60 °C as $3.9 \times 10^{-5}$ s. There are nine ethylene units in the fundamental Rouse unit,[45] so in a chain length typically equivalent to the alkanes, say $C_{250}$, $N$ will be equal to 13.9. A simple calculation involving the C−C bond length gives $b^2$ to be about $4 \times 10^{-19}$ m$^2$. Hence, $D_G$ is about $2.5 \times 10^{-17}$ m$^2$ s$^{-1}$. This compares with the diffusion coefficients within the crystal at the same temperature of $7 \times 10^{-21}$ and $8 \times 10^{-20}$ m$^2$ s$^{-1}$ (Table 6). This is physically reasonable, as one would expect diffusion within a crystal to be much slower than in the melt.

**Table 7. Diffusion Coefficients for Polyethylenes of Various Gel Fractions Obtained by Robertson et al.[12] from Fits to Eq 7**

| gel fraction | diffusion coefficient (nm$^2$ s$^{-1}$) |
|---|---|
| 0 | 0.033 |
| 0.78 | 0.0247 |
| 0.87 | 0.0183 |

The diffusion coefficients can also be compared with literature values for diffusion coefficients in polyethylene measured by the same NMR technique. Table 7 displays diffusion coefficients obtained by Robertson and co-workers[12] in a slow cooled, high-density polyethylene, some samples of which had been electron irradiated to form cross-links at the fold surface of the crystallites. They are the results of fits of eq 7 over the whole range of the relaxation. The crystallinity of each of these materials was measured, prior to irradiation, to be 76.9%. The diffusion coefficient for the unirradiated sample is less than that for quenched $C_{198}H_{398}$ (Table 5), a result of the presence of chain folds in the polyethylene. This coefficient is larger than that for the F1 alkanes (Table 5), a result of the exceptionally tight chain folding in the alkanes,[18] relative to that in polyethylene, representing a greater obstacle to the diffusion. As cross-links are added, they suppress the diffusion and the diffusion coefficients decrease to a value comparable with the F1 alkanes. This is consistent with cross-links being restricted from access to the crystals, forcing the onset of fold length fluctuating diffusion, as is here observed in the alkanes.

**Estimation of Tightness of Chain Folds.** The initial diffusion of chains has been ascribed to free diffusion before any constraints are "felt". Knowledge of the diffusion coefficient in this regime and of the time scale over which constraints become significant, $\tau_L$, allows the distance traveled by a chain before it encounters a constraint to be calculated. This distance corresponds to the length of a chain fold.

From Fick's Diffusion equation,[43] the displacement, $x$, of any chain can be found via

$$x = \sqrt{Dt} \tag{13}$$

Using a diffusion coefficient of 0.08 nm$^2$ s$^{-1}$ and a $t = \tau_L$ value of 30 s, this yields a displacement of 1.5 nm before constraints are "felt". Since this implies each stem can move by 1.5 nm, the fold would comprise some 24 bonds.

The more mobile, partially disordered material in the region of the chain folds is commonly described as the interphase between the crystalline and amorphous moieties.[39,41,46−48] The thickness of the interfacial phase predicted here, 1.5 nm, agrees well with literature values for interphase thicknesses in various polyethylenes. These values range between 3[41,47] and 5 nm.[39] The observation that alkane chain folds are somewhat tighter that those found in polyethylene is consistent with previous measurements suggesting tight and adjacently reeentrant folds in the alkanes.[18,19,27] An inter-

phase thickness of 1.5 nm is also consistent with a theoretical prediction[49] of 2.4 nm and a value of 1.2 nm derived from computer simulation.[50]

Twenty-four bonds represents some 8−12% of the chain for the various folded alkanes. Since the interphase is mobile enough to partially average the dipolar interaction,[39,48] it would have been interpreted as amorphous material from the $^1$H broadline NMR crystallinity measurements. It can be concluded from this that a large fraction of the 20% noncrystalline phase in the F1 alkanes was material associated with chain folding.

## Conclusions

$^{13}$C NMR progressive saturation measurements have been used to investigate longitudinal relaxation in the crystal phase of semicrystalline alkanes. Novel monodisperse, ultralong *n*-alkanes[17] were melt crystallized in such a way that they comprised crystals containing predominantly extended chains or exactly once-folded chains. The successful preparation of such bulk samples is ideal for an investigation of chain diffusion, allowing the constraints presented to chain diffusion to be identified precisely. The position, number, and lengths of the branches were precisely known. The lamellar thickness was uniform across any particular sample and could be varied by using alkanes of different molecular weights with confidence that the morphology was otherwise identical.

Following the work of Schmidt-Rohr and Spiess,[11] the longitudinal relaxation was not interpreted by a conventional $T_1$ process but rather with a solid-state chain diffusion process. Very high crystallinity was observed to impede the diffusion. Relaxations were measured from samples containing extended chain crystals and those containing folded chain crystals. It was found that chain folds represented a significant obstacle to the chain diffusion process, resulting in longer relaxation times. Surprisingly, the addition of a branch at the fold surface did not represent a further constraint to that posed by the fold itself. Since it was very unlikely that a branch could be dragged through a crystal, it was proposed that in all alkanes, linear and branched, material exchanges between the crystalline and amorphous phases not by sliding around the chain fold but rather by fluctuating the length of the chain fold. Taking this into account, a dual reptation time diffusion model was developed and shown to provide an excellent representation of the data over the full range of the relaxation. The diffusion coefficients produced were consistent both with previous measurements on polyethylene[12] and with the proposed mechanism of diffusion. The $C_{198}H_{398}$ and the branched samples displayed relaxation of 100% at long times. This is not attributed to entire chain stems escaping from the lamellae, which is unfeasible on thermodynamic grounds. We interpret this as a contribution from the intrinsic $T_1$ spin−lattice relaxation within the crystal.

The diffusion of polymer chains between the crystalline and amorphous phases of semicrystalline systems is an important process with respect to crystallization, lamellar thickening, and orienting phenomena. It could even be important for creep and crack propagation. However, this work has also revealed the insight into crystalline morphology which chain diffusion can provide. The fast relaxation of quenched $C_{198}H_{398}$ and the single reptation time nature of this relaxation showed that the crystal morphology comprised many, perhaps even largely, extended chains. Scattering and calorimetry both failed to reveal this. Further, the dual reptation time model provides a new method of measuring the thickness of the crystalline/amorphous interphase. Whereas much previous $^{13}$C longitudinal relaxation data have been interpreted through the conventional dipolar spin−lattice model, the establishment of physical transport of chains as the dominant relaxation mechanism can lead to stimulating new investigations in the field of ordering, structure, and dynamics in semicrystalline polymers.

**Acknowledgment.** The authors thank Dr. I. M. Hamley and Prof. A. J. Ryan for experimental assistance and helpful discussions on the X-ray scattering. We are also grateful to Dr. D. L. VanderHart for constructive comments regarding the $T_1$ relaxation. Financial support was provided by EPSRC, and samples were provided by the EPSRC Steering Group.

## References and Notes

(1) Ward, I. M.; Hadley, D. W. *An Introduction to the Mechanical Properties of Solid Polymers*, 2nd ed.; John Wiley and Sons: London, 1993.
(2) Takayanagi, M. *Mem. Fac. Eng., Kyushu Univ.* **1963**, *23*, 1−17.
(3) Illers, K. H.; H. Breuer, H. *J. Colloid Sci.* **1963**, *18*, 1−32.
(4) Ungar, G.; Keller, A. *Colloid Polym. Sci.* **1979**, *257*, 90−94.
(5) Narang, R. S.; Sherwood, J. N. *Mol. Cryst. Liq. Cryst.* **1980**, *59*, 167−174.
(6) Zerbi, G.; Piazza, R.; Holland-Moritz, K. *Polymer* **1982**, *23*, 1923−1928.
(7) Yamamoto, T.; Aoki, H.; Miyaji, S.; Nozaki, K. *Polymer* **1997**, *38*, 2643−2647.
(8) Yamamoto, T.; Nozaki, K. *Polymer* **1995**, *36*, 2505.
(9) Sumpter, B. G.; Noid, D. W.; Liang, G. L.; Wunderlich, B. *Adv. Polym. Sci.* **1994**, *116*, 29.
(10) Organ, S. J.; Ungar, G.; Keller, A. *J. Polym. Sci., Polym. Phys.* **1990**, *28*, 2365−2384.
(11) Schmidt-Rohr, K.; Spiess, H. W. *Macromolecules* **1991**, *24*, 5288−5293.
(12) Robertson, M. B.; Ward, I. M.; Klein, P. G.; Packer, K. J. *Macromolecules* **1997**, *30*, 6893−6898.
(13) Klein, P. G.; Robertson, M. B.; Driver, M. A. N.; Ward, I. M.; Packer, K. J. *Polym. Int.* **1998**, *47*, 76−83.
(14) Hu, J. Z.; Wang, W.; Bai, S.; Pugmire, R. J.; Taylor, C. M. V.; Grant, D. M. *Macromolecules* **2000**, *33*, 3359.
(15) Lee, K. S.; Wegner, G. *Makromol. Chem., Rapid Commun.* **1985**, *6*, 203−208.
(16) Bidd, I.; Holdup, D. W.; Whiting, M. C. *J. Chem. Soc., Perkin Trans. 1* **1987**, 2455−2463.
(17) Brooke, G. M.; Burnett, S.; Mohammed, S.; Proctor, D.; Whiting, M. C. *J. Chem. Soc., Perkin Trans. 1* **1996** 1635−1645.
(18) Ungar, G.; Stejny, J.; Keller, A.; Bidd, I.; Whiting, M. C. *Science* **1985**, *229*, 386−389.
(19) Boda, E.; Ungar, G.; Brooke, G. M.; Burnett, S.; Mohammed, S.; Proctor, D.; Whiting, M. C. *Macromolecules* **1997**, *30*, 4674−4678.
(20) Maxwell, A. S.; Unwin, A. P.; Ward, I. M. *Polymer* **1996**, *37*, 3293−3301.
(21) Becker, E. D.; Ferretti, J. A.; Gambhir, P. N. *Anal. Chem.* **1979**, *51*, 1413−1420.
(22) Wunderlich, B.; Cormier, C. M. *J. Polym. Sci., Part A-2* **1967**, *5*, 987−988.
(23) Bras, W.; Derbyshire, G. E.; Ryan, A. J.; Mant, G. R.; Felton, A.; Lewis, R. A.; Hall, C. J.; Greaves, G. N. *Nucl. Instrum. Methods Phys. Res.* **1993**, *A326*, 587−591.
(24) Lewis, R. A.; Sumner, I.; Berry, A.; Bordas, J.; Gabriel, A.; Mant, G.; Parker, B.; Roberts, K.; Worgan, J. *Nucl. Instrum. Methods* **1988**, *A273*, 773−777.
(25) Blundell, D. I. *Polymer* **1978**, *19*, 1258−1266.
(26) Ballon, J.; Comparat, V.; Pouxe, J. *Nucl. Instrum. Methods* **1983**, *217*, 213−216.
(27) Organ, S. J.; Keller, A.; Hikosaka, M.; Ungar, G. *Polymer* **1996**, *37*, 2515−2524.
(28) Hay, J. N.; Zhou, X.-Q. *Polymer* **1993**, *34*, 1002−1005.

(29) Hoffman, J. D.; Davis, G. T.; Lauritzen, J. I. In *Treatise on Solid State Chemistry*; Hannay, Ed.; Plenum Press: New York, 1976; Vol. 3, pp 497−605.
(30) Mandelkern, L.; Prasad, A.; Alamo, R. G.; Stack, R. M. *Macromolecules* **1990**, *23*, 3696−3700.
(31) Flory, P. J. *J. Chem. Phys.* **1949**, *17*, 223−240.
(32) Ungar, G.; Zeng, X. B.; Brooke, G. M.; Mohammed, S. *Macromolecules* **1998**, *31*, 1875−1879.
(33) Ungar, G.; Keller, A. *Polymer* **1986**, *27*, 1835−1844.
(34) Balta-Calleja, F. J.; Vonk, C. G. *X-ray Scattering of Synthetic Polymers*; Elsevier: Amsterdam, 1989; pp 254−256, 272.
(35) Driver, M. A. N. PhD Thesis, University of Leeds, 1999; Chapter 4.
(36) Moller, M.; Cantow, H.-J.; Drotloff, H.; Emeis, D.; Lee, K.-S.; Wegner, G. *Makromol. Chem.* **1986**, *187*, 1237−1252.
(37) Kitamaru, R.; Horii, F.; Zhu, Q.; Bassett, D. C.; Olley, R. H. *Polymer* **1994**, *35*, 1171−1181.
(38) Axelson, D. E.; Mandelkern, L.; Popli, R.; Mattieu, P. *J. Polym. Sci., Polym. Phys.* **1983**, *21*, 2319−1335.
(39) Eckmann, R. R.; Henrichs, P. M.; Peacock, A. J. *Macromolecules* **1997**, *30*, 2474−2481.
(40) Cheng, J.; Fone, M.; Reddy, V. N.; Schwartz, K. B.; Fisher, H. P.; Wunderlich, B. *J. Polym. Sci., Polym. Phys.* **1994**, *32*, 2683.
(41) Kitamaru, R.; Horii, F.; Murayama, K. *Macromolecules* **1986**, *19*, 636−643.
(42) VanderHart, D. L., personal communication.
(43) Crank, J. *The Mathematics of Diffusion*; Clarendon Press: Oxford, England, 1975; Chapter 4.
(44) Doi, M.; Edwards, S. F. *The Theory of Polymer Dynamics*; Clarendon Press: Oxford, England, 1986; Chapter 6.
(45) Brereton, M. G.; Ward, I. M.; Boden, N.; Wright, P. *Macromolecules* **1991**, *24*, 2068−2074.
(46) Kitamaru, R.; Nakaoki, T.; Alamo, R. G.; Mandelkern, L. *Macromolecules* **1996**, *29*, 6847−6852.
(47) Kuwabara, K.; Hoji, H.; Horii, F.; Bassett, D. C.; Olley, R. H. *Macromolecules* **1997**, *30*, 7516−7521.
(48) Kristiansen, P. E.; Hansen, E. W.; Pederson, B. *J. Phys. Chem. B* **1999**, *103*, 3552−3558.
(49) Flory, P. J.; Yoon, D. Y.; Dill, A. *Macromolecules* **1984**, *17*, 862−868.
(50) Balijepalli, S.; Rutledge, G. C. *J. Chem. Phys.* **1998**, *109*, 6523−6526.

MA000571B